Hydration, Microstructure and Compressive Strength Development of Seawater-mixed Calcium Sulphoaluminate Cement-based Systems

Ting ZHANG [1, 2], **Ditao NIU** [1, 2] *, **Chaofei LI** [3]

[1] *State Key Laboratory of Green Building in Western China of Xian University of Architecture & Technology, Xi'an 710055, China*
[2] *College of Civil Engineering, Xi'an University of Architecture & Technology, Xi'an 710055, China*

In-depth understanding of the calcium sulphoaluminate (CSA) cement, a type of environment-friendly cement, is essential for its wide application in engineering practice. Partial replacement of CSA by alternative alumina-rich powders has significant potential in the production of cost-effective CSA cement. In this work various supplementary cementitious materials (SCMs) including slag, metakaolin and silica fume with different replacement levels were added into CSA cement, and mixing with seawater, to prepare paste and concrete specimens. The development of hydration products in the paste specimens was characterized by X-ray diffraction and Thermogravimetric analysis. The pore structures of the seawater-mixed paste specimens obtained from mercury intrusion porosimetry tests, along with the pH value and free chloride content in the pore solution, were analyzed. Results show that various SCMs have significantly different effects on the pore solution chemistry, hydration and microstructural formation of the seawater-mixed CSA cement, resulting in different mechanical behavior and durability properties. The results of this work are helpful for the development of cost-effective CSA cement-based concrete used in marine constructions.

Keywords: calcium sulphoaluminate cement, supplementary cementitious materials, seawater, microstructure, strength.

1. INTRODUCTION

Calcium sulphoaluminate (CSA) cement has drawn considerable attention since its first development in the 1970s. The interest in utilization of the CSA cement lies in its superior performances such as fast setting, high early strength, low permeability, high resistance to frost damage, etc. [1–5]. The CSA clinker is derived by calcination of pure chemicals and/or commercially available minerals like gypsum, bauxite and limestone. The calcination temperature is in the range of 1250–1350 °C, approximately 200 °C lower than that of Portland cement clinker. The CSA clinker has a better grindability and shows less energy consumption and less CO_2 emission [6, 7]. CSA cement is produced by mixing the CSA clinker with gypsum ($C\hat{S}H_2$) or anhydrite ($C\hat{S}$). The properties of CSA cement, e.g. setting time and shrinkage, can readily be adjusted by changing the gypsum content [8]. Standardization of various kinds of CSA cement usually follows from Eq. 1:
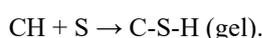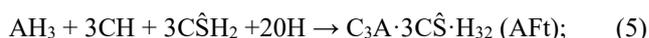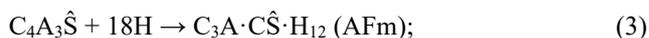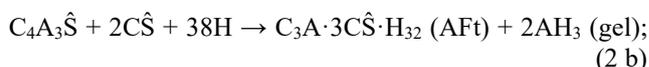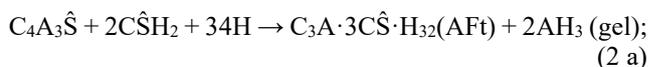
$$C_G = 0.13 M \, A_c / \bar{S}, \tag{1}$$

where C_G is the gypsum-clinker mass ratio; M is the gypsum-ye'elimite molar ratio; A_c and $\bar{S}$ are the mass percentage of the ye'elimite in the clinker and the SO_3 in the gypsum (or anhydrite), respectively.

Ye'elimite ($C_4A_3\hat{S}$ in cement notation) is the major component of CSA cement. The Al^{3+} within ye'elimite can be partially replaced by Fe^{3+}. Other phases including belite (known as larnite C_2S occasionally), ferrite phases (C_4AF) and mayenite ($C_{12}A_7$) are also present in the CSA cement. The belite hydrates limited in the first 7 d and up to a degree

about 5–40 % at 28 d [9].

The main hydration products of ye'elimite ($C_4A_3\hat{S}$) are monosulphoaluminate (AFm), aluminium hydroxide (AH_3) and ettringite (AFt) (Eq. 2 a and b) [10]. Other minor hydrates like CAH_{10} or C_4AH_{13} can be present depending on the temperature and minerology of the CSA cement [11]. With the formation of AH_3, the hydrated particles are bound together. The reaction according to Eq. 3 takes place when the calcium sulfate is insufficient [12]. The belite reacts with water to form C-S-H gels and calcium hydroxide (CH) (Eq. 4). The reaction as provided in Eq. 5 occurs at later age. AFt is expansive owing to its large specific volume. The addition of supplementary cementitious materials may lead to the occurrence of pozzolanic reaction (Eq. 6). The AFt or AFm enables to bind a large amount of heavy metals [8].

$$C_4A_3\hat{S} + 2C\hat{S}H_2 + 34H \rightarrow C_3A \cdot 3C\hat{S} \cdot H_{32}(AFt) + 2AH_3 \text{ (gel)}; \tag{2 a}$$

$$C_4A_3\hat{S} + 2C\hat{S} + 38H \rightarrow C_3A \cdot 3C\hat{S} \cdot H_{32} \text{ (AFt)} + 2AH_3 \text{ (gel)}; \tag{2 b}$$

$$C_4A_3\hat{S} + 18H \rightarrow C_3A \cdot C\hat{S} \cdot H_{12} \text{ (AFm)}; \tag{3}$$

$$C_2S + 2H \rightarrow \text{C-S-H (gel)} + CH; \tag{4}$$

$$AH_3 + 3CH + 3C\hat{S}H_2 + 20H \rightarrow C_3A \cdot 3C\hat{S} \cdot H_{32} \text{ (AFt)}; \tag{5}$$

$$CH + S \rightarrow \text{C-S-H (gel)}.$$

A higher ratio of AFt/AFm is found with a rise in the gypsum content [13, 14]. The presence of AFt is influenced basically by the hydration temperature. Mehta [15] stated that AFt is stable at 65 °C while decomposes at around

---

* Corresponding author. Tel.: +86-29-82205506; fax: +86-29-82205506.
E-mail address: *niuditao@163.com* (D. Niu).

93 °C in OPC pastes. A lower decomposition temperature of the AFt in CSA cement pastes was found by Berger et al. [14]. A rapid transition of AFt to AFm takes place with elevated temperature from 50 to 80 °C [14]. As a major hydration product, the AFt substantially contributes to the superior properties of CSA cement, such as high early-age strength, low shrinkage or even expansion. These properties, however, largely depend on conditions of the AFt formation [13]. The amorphous hydrates, C-S-H and AH_3 gels, play an important part in the densified microstructure at later age [16]. Production of the CSA cement requires a large amount of high-quality alumina source. This limits an abroad application of the CSA cement in engineering practice. Great opportunities lie in partial replacement of the CSA by supplementary cementitious materials (SCMs). Additions of SCMs will affect the hydration and microstructural formation, due to changes of the chemical composition and particle size distribution. Tan et al. [17] demonstrated that lithium slag can be added into CSA cement to promote the early strength. Ma et al. [18] found an increase of compressive strength for the CSA cement concrete with nano-SiO_2. Bullerjahn et al. [19, 20] analyzed the chemical shrinkage after ye'elimite hydration and explained as due to recrystallization of the amorphous phases. Wang et al. [21] found a homogeneous CSA cement paste matrix when curing under 20 °C. At long ages, the CSA cement with 5 % limestone powder presents a similar pore structure as that formed by the pure CSA cement [22]. The limestone filler enables to stabilize AFt and minimize the formation of AFm [23].

There have, however, been few studies on the CSA cement systems blended with reactive pozzolanic materials. One reason is related to complexity of the microstructure formed. In addition, little research is available regarding the performance of CSA cementitious systems prepared with seawater. Owing to the scarcity of fresh water, in particular considering the convenience and economic practicality in the marine engineering, utilization of seawater and reactive SCMs has become a prevailing trend.

In this work a range of SCM-CSA binary cementitious samples, mixed with seawater, was prepared. The pore structures measured from mercury intrusion porosimetry and the hydration products identified by X-ray diffraction and thermogravimetric analysis were investigated. The pH and free chloride content in the pore solution, as well as the microstructure-strength relationship, were analyzed.

2. EXPERIMENTAL

2.1. Raw materials and samples

The raw materials were calcium sulphoaluminate (CSA) cement, silica fume (SF), ground granulated blast furnace slag (GS) and metakaolin (MK). The chemical composition by X-ray fluorescence is given in Table 1.

Table 1. Chemical composition (wt%) of the raw materials

	SiO_2	Al_2O_3	Fe_2O_3	CaO	MgO	SO_3
CSA	6.1	16.4	2.0	49.2	1.4	20.6
MK	49.1	43.9	3.1	1.6	0.1	0.1
SF	94.9	0.5	0.2	1.3	0.2	0.1
GS	32.5	17.9	0.9	32.6	6.0	2.8

The mineral compositions of the CSA clinker, by quantitative X-ray diffraction analysis, were 60.12 % for $C_4A_3\hat{S}$, 24.12 % for C_2S, 6.23 % for C_4AF and 4.25 % for mayenite ($C_{12}A_7$). The mean particle size d_m was 2.95 μm, 4.77 μm, 11.46 μm and 13.23 μm for MK, SF, GB and FA, respectively.

Different binders (Table 2) were mixed with seawater for casting paste specimens. A fixed water-to-binder-ratio (w/b) of 0.45 was used. The powders and seawater were mixed at a low speed for 1 min and at a high speed for 2 min. The paste mixtures were then poured into plastic bottles, and vibrated continuously to remove the air bubbles that were possibly introduced during the mixing process. The bottles with paste mixtures were sealed and rotated for 24 h to avoid segregation before they were cured at 20 ± 1 °C. Cement concrete specimens were prepared for compressive strength tests. All concrete specimens were made with the same amount of fine/coarse aggregates, but varied with binders. At the ages of 1 h, 7 h, 1 d, 7 d and 28 d, the paste and concrete specimens were carried out with various measurements.

The composition of the seawater, collected from the South China Sea, is listed in Table 3. The initial and final setting time of all mixtures were measured by a Vicat needle following ASTM C191 [24]. The results are given in Table 2. The blended mixtures have longer time of initial setting due to the slower hydration as compared to the CSA.

Table 2. Binder mixtures and setting time (min)

Binders	CSA	MK	SF	GS	Initial setting	Final setting
CSA	100 %				43	72
MK5	95 %	5 %			58	77
MK10	90 %	10 %			55	70
MK15	85 %	15 %			50	61
SF3	97 %		3 %		75	84
SF6	94 %		6 %		73	81
SF10	90 %		10 %		63	69
GS10	90 %			10 %	74	82
GS20	80 %			20 %	69	75
GS30	70 %			30 %	66	74

Table 3. Seawater composition of the south China sea

Elements	Cl	Na	Mg	S	Ca	K
Mass, g/kg	19.39	10.79	1.27	2.77	0.41	0.40

2.2. Pore structure by MIP

Mercury intrusion porosimetry (MIP) was applied for characterizing the pore structure of various paste mixtures. The paste specimens were split into pieces (around 1 cm³) and then immersed in liquid nitrogen to stop further hydration and subsequently moved to a freeze-drier under vacuum and at –24 °C [25]. After the mass loss was below 0.01 % per day, the paste specimens can be used for MIP tests. The applied pressure P (MPa) and pore diameter d (μm) can be described with the Washburn equation:

$$d = (-4\gamma cos\theta)/P, \tag{7}$$

where γ and θ are the surface tension of mercury and the contact angle between mercury and pore wall, respectively.

2.3. Characterization of hydration products

X-Ray diffraction (XRD) was employed to identify the main crystalline phases in various paste mixtures. Rigaku-D/max2550VB3 with Cu Kα radiation (λ = 1.541 Å), operating at 40 kV and 30 mA, was used. The scanning was conducted over a 2θ range of 5 – 70 °C with step size of 0.03°. The paste specimens after freeze-drying were ground into powders while using ethyl alcohol to avoid contamination of moisture or carbonation. The crystalline phases of the powered samples were identified after comparing with the standards of International Centre for Diffraction Data.

Thermogravimetric analysis (TGA) was performed to identify the chemically bound water. A NETZSCH STA (TG-DTA-DSC) 449 F3 Jupiter was used. The powdered sample was heated from 40 to 1000 °C with a heating rate of 10 °C/min under the argon atmosphere.

2.4. Pore solution chemistry

Chloride content and pH are the main factors affecting the reinforcement corrosion of concrete structures [26, 27]. Cylindrical paste specimens (φ 50 × 100 mm) cured at ages of 1 d, 7 d and 28 d were compressed under high pressure by following the method proposed by Barneyback and Diamond [28]. The obtained pore solutions were filtered using a 0.45 μm pore size filter to remove the residual particles, and then performed with pH measurement (using a Metrohm 6.0255.100 Profitrode electrode) and free chloride content measurement (using potentiometric titration [29]). Buffer solutions of pH at 7, 10, 11, 12 and 13 were used to calibrate the Metrohm electrode.

2.5. Compressive strength

A testing machine with a capacity of 500 kN was used for compressive strength tests. Concrete specimens (40 × 40 × 160 mm) were cast and moist-cured after 1 d, 3 d, 7 d and 28 d. A loading rate of 2.4 kN/s was applied for the strength tests. For each mixture three parallel measurements were carried out and the average was used for report.

3. RESULTS AND DISCUSSION

3.1. Mineralogy by XRD

The hydration products of various cement pastes with and without SCMs were characterized by XRD. The results are presented in Fig. 1. The products including C-S-H and AH₃ gels can hardly be seen in the XRD pattern owing to their poor crystallinity. A phase with its amount less than 5 % is difficult to be identified as well [30]. The main components of the raw CSA cement, ye'elimite and anhydrite, are clearly observed (Fig. 1 a). Both contents are significantly decreased with hydration in the first 7 h, followed by a gradual decrease afterwards. The amount of AFt increases with age. The amount of belite and mayenite is not clearly decreased and the amount of calcite stays nearly constant in the first 7 d.

By adding SF (Fig. 1 b) the ye'elimite is considerably reduced after 1 d hydration and the AFt is increased, irrespective of the SF replacement level from 3 % to 10 %. The amount of belite is decreased and a larger decrease corresponds to a higher replacement of SF from 3 % to 6 %. This is a result of the pozzolanic reaction (Eq. 6) which accelerates the belite hydration (Eq. 4). There is little difference in the diffraction peaks between SF6 and SF10. Of particular interest is that more anhydrite is found in the SF-blended binders than in the CSA binder. This is due to the fact that the CH preferably reacts with SiO_2, rather than with AH_3, to form C-S-H gels and the reaction (Eq. 5) is thus impeded. A higher amount of mayenite is found after incorporation of the SF.

Similar observations are found between GS-blended binders and SF-blended binders. As seen in Fig. 1 c, the amounts of ye'elimite and belite are substantially decreased. The anhydrite, AFt and mayenite are increased while the calcite is not significantly altered. Different roles of MK in the hydration is found based on the pattern shown in Fig. 1 d. By substituting CSA with MK, from 5 % to 15 %, all peaks corresponding to various solid phases are not much different, except the peak for anhydrite, which is tremendously higher in the MK-blended binders than in the CSA binder.

It appears that the hydration of ye'elimite proceeds to a similar degree but the reaction of anhydrite is significantly impeded after adding MK, regardless of the replacement level. CH and gypsum are not found in the CSA-based cementitious systems with and without blends, as can be seen from all the XRD patterns shown in Fig. 1.

3.2. Mass loss by TGA

Fig. 2 shows the TG-curves for different cementitious systems hydrated from 1 h to 28 d.
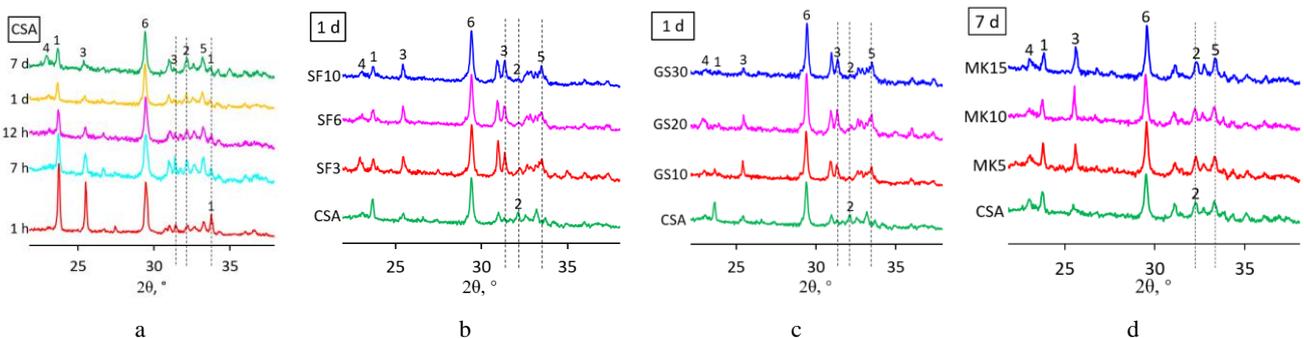
Fig. 1. XRD patterns of CSA and blended cement paste specimens: a – age from 1 h to 7 d; b – effect of SF, age = 1 d; c – effect of GS, age = 1 d; d – effect of MK, age = 7 d. Notes: 1 – Ye'elimite (C₄A₃Ŝ); 2 – Belite (C₂S); 3 – Anhydrite; 4 – Ettringite (AFt); 5 – Mayenite (C₁₂A₇); 6 – Calcite
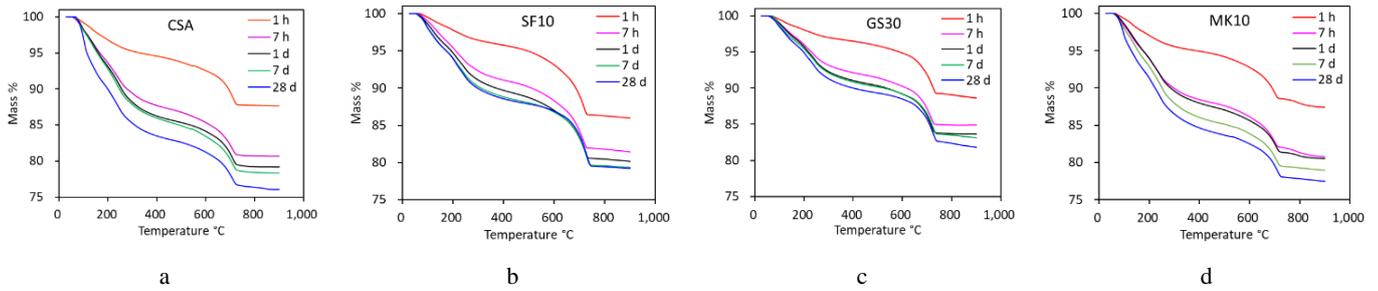
Fig. 2. TG-curves of CSA and blended cement paste specimens from 1 h to 28 d

The mass loss with elevated temperature is mainly owing to the release of water and carbon oxide (in the temperature range 600–730 °C). The TG-curves confirm the evolution of phase assemblages as already observed in the XRD patterns. The mass loss generally increases with age from 1 h to 28 d. Such increase is particularly pronounced in the first 7 h, indicating a rapid and intensive hydration process in the CSA-based binders. Relative to the mass loss at 28 d, the mass loss of the first 7 h accounts for 88.5 %, 89.4 %, 83.1 % and 83.1 % for binders CSA, SF10, GS30 and MK10, respectively.

After 1 h hydration (Fig. 3 a), the CSA binder has larger total mass loss than the GS-blended binders, but smaller than the SF-blended binders. With different replacement levels, the binders GS10, GS20 and GS30 have similar total mass loss. This finding holds also for the SF-blended binders SF3, SF6 and SF10. A higher substitution of CSA by GS from 10 % to 30 %, after 7 d hydration (Fig. 3 b), results in a larger total mass loss. When CSA is partially replaced by SF (Fig. 3 c), the total mass loss is increased at a replacement level of 3 %. A slight decrease in the total mass loss is found with a rise in the SF replacement level

from 3 % to 6 %. The total mass loss increases again when the SF replacement level is further increased to 10 %. By including 5 % MK (Fig. 3 d), the TG-curves of MK5 differs slightly from that of CSA. For higher replacement levels, binders MK10 and MK15 exhibit similar mass loss against temperature and both show larger total mass loss than MK5.

3.3. Pore structure

The results of cumulative pore volumes and their differential curves for different binders after 28 d hydration, obtained from MIP tests, are provided in Fig. 4. The total pore volume is the highest in GS30, followed by SF10, CSA and MK15 (Fig. 4 a). A main peak is present for the GS-blended binder GS30 (Fig. 4 b). The diameter corresponding to the main peak is defined as critical pore diameter. Despite of a higher total pore volume, the CSA has a finer pore size distribution than the MK15. The low total pore volume of MK15 can be partly related to the high reactivity of MK and partly related to its small particle sizes (d_m = 2.95 µm).
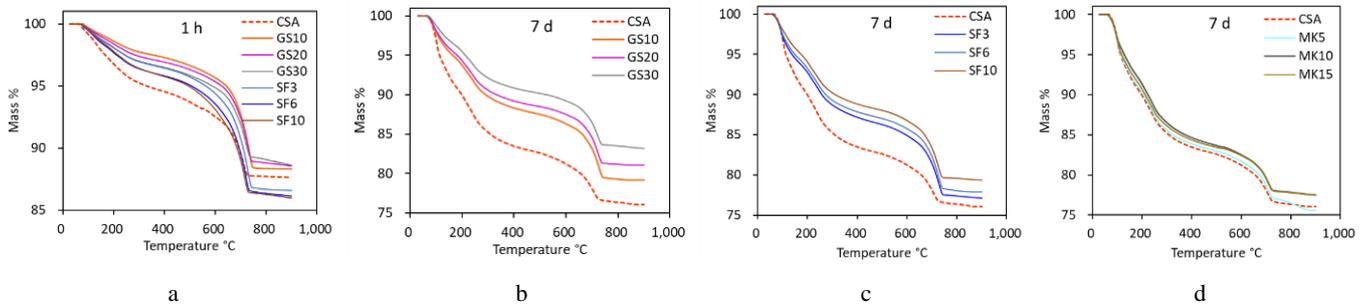
Fig. 3. TG-curves of CSA and blended cement paste specimens hydrated at 1 h and 7 d
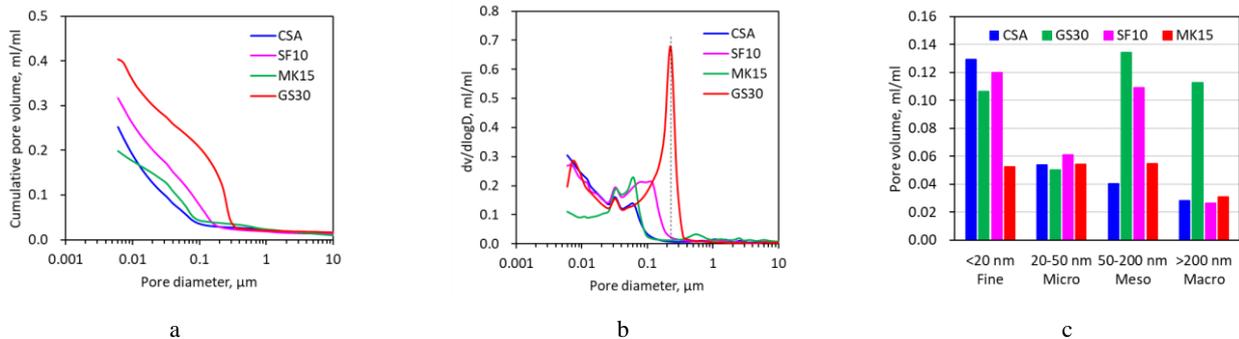
Fig. 4. Pore structure of CSA and blended cement paste specimens at 28 d: a – cumulative pore volume; b – differential curve; c – volume of four different pore size groups

For a further examination, the pore family is categorized into four groups: fine pores (< 20 nm), micro pores (20 – 50 nm), meso pores (50 – 200 nm) and macro pores (> 200 nm). The volume of each pore group calculated according to the data of Fig. 4 a is provided in Fig. 4 c. For the macro pore group (> 200 nm), the mixtures CSA, SF10 and MK15 have similar volume, which is however four times smaller than that of the mixture GS30. An abrupt increase in the pore volume of the mixture SF10 is found from the macro to the meso pore group. The volume of the meso pores shows an obvious ascending order in the mixtures CSA, MK15, SF10 and GS30. The volume of the micro pores differs slightly between different mixtures. The fine pores are less in the mixture MK15 than in the other mixtures CSA, GS30 and SF10.

3.4. PH and chloride content

The pH of the pore solution in hydrated ordinary Portland cement (OPC) based systems is normally in the range 12.5 – 13.8 [31]. The lower limit of pH = 12.5 is related to the intrinsic ingredient of the cement pore solution, which is often saturated with respect to Portlandite (CH). The presence of alkalis Na^+ and K^+ enables to increase the pH to a level above 12.5. The reinforcement is no longer protected from corrosion once the pH is below approximately 10 [32].

As indicated in Table 4, the pH of CSA-based mixtures are all below 12.5, suggesting that the hydration products of the CSA-based systems comprise limited amount of soluble Ca^{2+} and the pore solution is not saturated with respect to CH. This can be confirmed by the results of XRD (Fig. 1) and TG (Fig. 2) that little CH is found. The addition of MK (5 – 15 %) increases the pH of the CSA system in the first 7 d of hydration, but decreases the pH at 28 d. Substitution of CSA by SF (3 – 10 %) or by GS (10 – 30 %) decreases the pH in the first 28 d. Interestingly to note that the pH is decreased by comparing the data between 1 d and 28 d. This can be related to the increased amount of C-S-H gels that adsorb alkalis from the pore solution.

For different binders the free chloride content is in the range 1.494 – 2.523 for 1 d and 1.074 – 3.175 for 28 d (see Table 4).

Table 4. pH and chloride content in the pore solution of paste mixtures mixed with seawater

	pH			Chloride content, mol/L		
	1 d	7 d	28 d	1 d	7 d	28 d
CSA	11.19	11.28	11.11	1.961	2.195	3.175
MK5	11.42	11.32	10.98	2.216	1.568	2.764
MK10	11.38	11.40	11.10	2.523	2.012	2.228
MK15	11.21	11.38	10.96	1.927	1.664	2.003
SF3	10.81	10.92	10.74	1.622	1.585	2.108
SF6	10.79	10.93	10.81	1.887	1.193	2.09
SF10	10.79	10.91	10.94	1.559	1.183	2.176
GS10	10.90	11.05	10.83	2.100	1.393	1.574
GS20	11.14	11.12	10.51	1.494	1.473	1.528
GS30	11.18	11.14	10.35	1.554	1.013	1.294

The free chloride content obviously increases with age for CSA. In the 1 d hydration, the chlorides have a high capability to combine the alumina phases. As ongoing hydration, the alumina phases react preferably with the sulfate phases to form a more stable product of ettringite. As a consequence, the bound chlorides are released resulting in a higher free chloride content in the pore solution.

The free chloride content decreases in the period 1 – 7 d while increases in the period 7 – 28 d. This is resonable. The MK reacts with CH and concurrently the product AH_3 will chemically combine the chlorides, resulting in a lower amount of free chlorides in the pore solution. This finding holds also for the SF-blended mixtures (SF3, SF6 and SF10) and GS-blended mixtures (GS10, GS20 and GS30).

3.5. Compressive strength

The results of the compressive strength development from 1 d to 28 d for CSA cement concrete specimens with and without blends are presented in Table 5. All values are based on measurements of three replicates. The standard deviation of the strength value with respect to the average was within 8 % for all mixtures. In most cases the compressive strength is higher with age, due to continuous hydration and associated precipitation of hydration products. Occasionally, at ages of 3 – 7 d, a slight decrease in the compressive strength can be found, which is attributable to the formation of expansive ettringite at later age (Eq. 5) and subsequently resulting in cracking. At 28 d, however, the compressive strength is much higher than that in the first 7 d. This holds for all mixtures tested.

Table 5. Evolution of compressive strength (MPa) of seawater-mixed CSA-based concretes

Mixtures	1 d	3 d	7 d	28 d
CSA	52.17	58.67	75.08	77.17
MK5	54.50	65.92	80.73	85.33
MK10	44.92	51.75	58.75	65.58
MK15	48.00	48.83	55.33	69.75
SF3	52.67	54.42	52.58	64.13
SF6	51.52	50.58	50.33	63.50
SF10	50.50	51.63	51.67	61.42
GS10	39.75	45.50	46.83	61.17
GS20	40.17	52.67	47.17	65.08
GS30	36.42	40.33	40.17	49.17

With addition of 5 % MK (MK5), the compressive strength is obviously higher than that of the pure CSA at ages from 1 d to 28 d. For a higher addition, viz. MK10 and MK15, the compressive strength decreases considerably and it is even lower than that of the pure CSA. Between MK10 and MK15, the values of compressive strength are similar from 1 d to 28 d. These observations coincide well with the hydration results, as reflected by the TG-curves in Fig. 3 d. The presence of 3 % SF (SF3) results in the highest compressive strength, compared to the higher replacement levels of 6 % (SF6) and 10 % (SF10). By incorporating 20 % of GS, the mixture GS20 has higher compressive strength, compared with the replacement levels of 10 % and 30 %. After 7 d, the increase of compressive strength is limited for the CSA binder, but is significant for the blended binders. The compressive strength presents an ascending order in the binders CSA, MK15, SF10 and GS30. This is consistent with the same ascending order for the total mass loss in their TG-curves (Fig. 2). In general, the compressive strength at 3 d reaches approximately 80 % of that at 28 d.

A pore structure with finer pore size distribution tends

to exhibit a higher compressive strength [33, 34]. As already illustrated in Fig. 4 c, the volume of macro pores (> 200 nm) is the largest in the mixture GS30, which is much higher than that of the other three mixtures. The volume of meso pores (50 – 200 nm) shows a clear descending order in the mixtures GS30, SF10, MK15 and CSA, providing a solid explanation for the ascending order in the compressive strength of these mixtures.

4. CONCLUSIONS AND PROSPECTS

From the experimental results the main conclusions can be summarized as follows:

1. Hydration of the calcium sulphoaluminate (CSA) cement with seawater is pronounced in the first 7 h and becomes slow afterwards. Calcium hydroxide and gypsum are not found in the hardened CSA cementitious systems with and without SCMs.

2. For seawater-mixed CSA cementitious systems, the pH is below 11.5 and it is lower at 28 d than at 1 d. A small amount of supplementary cementitious materials (SCMs) can substantially affect the hydration and microstructural formation. The free chloride content is significantly decreased with the addition of SCMs, and particularly with slag.

3. The initial setting time of CSA cement is prolonged with the addition of slag, silica fume or metakaolin. The effects of SCMs on the compressive strength are consistent with their role in the chemically bound water content. The compressive strength increases quickly at the early age, but develops slowly after 7 d.

Combined application of CSA cement, silica fume and metakaolin (or slag) has a significant potential in promoting the strength development of CSA cement, and this is a subject well worthy to be carried out in future.

REFERENCES

1. **Popescu, C.D., Muntean, M., Sharp, J.H.** Industrial trial production of low energy belite cement *Cement and Concrete Composites* 25 (7) 2003: pp. 689 – 693. https://doi.org/10.1016/S0958-9465(02)00097-5

2. **Wang, Y., Su, M., Zhang, L.** Sulphoaluminate Cement (in Chinese), Beijing Industrial University Press, Beijing, 1999.

3. **Tian, H., Kong, X., Su, T., Wang, D.** Comparative study of two PCE superplasticizers with varied charge density in Portland cement and sulfoaluminate cement systems *Cement and Concrete Research* 115 2019: pp. 43 – 58.
https://doi.org/10.1016/j.cemconres.2018.10.003

4. **García-Maté, M., De la Torre, A.G., León-Reina, L., Aranda, M., Santacruz, I.** Hydration studies of calcium sulfoaluminate cements blended with fly ash *Cement and Concrete Research* 54 2013: pp. 12 – 20.
https://doi.org/10.1016/j.cemconres.2013.07.010

5. **Wang, Y.M., Su, M.Z., Zhang, L.** Sulphoaluminate cement, Peking University Press, Peking, China, 1990.

6. **Gartner, E.** Industrially interesting approaches to "low-CO₂" cements *Cement and Concrete Research* 34 (9) 2004: pp. 1489 – 1498.
https://doi.org/10.1016/j.cemconres.2004.01.021

7. **Coppola, L., Coffetti, D., Crotti, E.** Use of tartaric acid for the production of sustainable Portland-free CSA-based mortars *Construction and Building Materials* 171 2018: pp. 243 – 249.
https://doi.org/10.1016/j.conbuildmat.2018.03.137

8. **Zhang, L.** Microstructure and performance of calcium sulfoaluminate cement, PhD Thesis, Aberdeen University, UK, 2000.

9. **Kasselouri, V., Tsakiridis, P., Malami, C.H., Georgali, B., Alexandridou, C.** A study on the hydration products of a non-expansive sulfoaluminate cement *Cement and Concrete Research* 25 (8) 1995: pp. 1726 – 1736.
https://doi.org/10.1016/0008-8846(95)00168-9

10. **Lan, W., Glasser, F.P.** Hydration of calcium sulphoaluminate cements *Advances in Cement Research* 8 1996: pp. 127 – 134.
https://doi.org/10.1680/adcr.1996.8.31.127

11. **Winnefeld, F., Lothenbach, B.** Hydration of calcium sulfoaluminate cements – experimental findings and thermodynamic modelling *Cement and Concrete Research* 40 (8) 2010: pp. 1239 – 1247.
https://doi.org/10.1016/j.cemconres.2009.08.014

12. **Winnefeld, F., Barlag, S.** Calorimetric and thermogravimetric study on the influence of calcium sulfate on the hydration of ye'elimite *Journal of Thermal Analysis and Calorimetry* 101 (3) 2010: pp. 949 – 957.
https://doi.org/10.1007/s10973-009-0582-6

13. **Bizzozero, J., Gosselin, C., Scrivener, K.L.** Expansion mechanisms in calcium aluminate and sulfoaluminate systems with calcium sulfate *Cement and Concrete Research* 56 2014: pp. 190 – 202.
https://doi.org/10.1016/j.cemconres.2013.11.011

14. **Berger, S., Coumes, C., Le Bescop, P., Damidot, D.** Influence of a thermal cycle at early age on the hydration of calcium sulphoaluminate cements with variable gypsum contents *Cement and Concrete Research* 41 (2) 2011: pp. 149 – 160.
https://doi.org/10.1016/j.cemconres.2010.10.001

15. **Mehta, P.** Stability of ettringite on heating *Journal of the American Ceramic Society* 55 (1) 1972: pp. 55 – 56.
https://doi.org/10.1111/j.1151-2916.1972.tb13403.x

16. **Telesca, A., Marroccoli, M., Pace, M.L., Tomasulo, M., Valenti, G.L., Monteiro, P.** A hydration study of various calcium sulfoaluminate cements *Cement and Concrete Composites* 53 2014: pp. 224 – 232.
https://doi.org/10.1016/j.cemconcomp.2014.07.002

17. **Tan, H.B, Zhang, X., He, X.Y, Guo, Y., Deng, X., Su, Y., Yang, J., Wang, Y.** Utilization of lithium slag by wet-grinding process to improve the early strength of sulphoaluminate cement paste *Journal of Cleaner Production* 205 2018: pp. 536 – 551.
https://doi.org/10.1016/j.jclepro.2018.09.027

18. **Ma, B., Li, H., Mei, J., Li, X.** Influence of nano-SiO₂ addition on properties of sulphoaluminate cement based material *Journal of Wuhan University of Technology-Materials Science Edition* 32 (1) 2017: pp. 106 – 112.
https://doi.org/10.1007/s11595-017-1567-0

19. **Bullerjahn, F., Boehm-Courjault, E., Zajac, M., Ben Haha, M., Scrivener, K.L.** Hydration reactions and stages of clinker composed mainly of stoichiometric ye'elimite *Cement and Concrete Research* 116 2019: pp. 120 – 133.

https://doi.org/10.1016/j.cemconres.2018.10.023

20. **Bullerjahn, F., Skocek, J., Haha, M.B., Scrivener, K.** Chemical shrinkage of ye'elimite with and without gypsum addition *Construction and Building Materials* 200 2019: pp. 770 – 780.
https://doi.org/10.1016/j.conbuildmat.2018.12.170

21. **Wang, P., Li, N., Xu, L.** Hydration evolution and compressive strength of calcium sulphoaluminate cement constantly cured over the temperature range of 0 to 80 °C *Cement and Concrete Research* 100 2017: pp. 203 – 213.
https://doi.org/10.1016/j.cemconres.2017.05.025

22. **Ma, J., Yu, Z., Ni, C., Shi, H., Shen, X.** Effects of limestone powder on the hydration and microstructure development of calcium sulphoaluminate cement under long-term curing *Construction and Building Materials* 199 2019: pp. 688 – 695.
https://doi.org/10.1016/j.conbuildmat.2018.12.054

23. **Pelletier-Chaignat, L., Winnefeld, F., Lothenbach, B., Müller, C.J.** Beneficial use of limestone filler with calcium sulphoaluminate cement *Construction and Building Materials* 26 (1) 2012: pp. 619 – 627.
https://doi.org/10.1016/j.conbuildmat.2011.06.065

24. ASTM C191 – 19. Standard test methods for time of setting of hydraulic cement by Vicat needle. ASTM International, West Conshohocken, PA, 2019, www.astm.org.

25. **Zhang, Y., Yang, Z., Ye, G.** Dependence of unsaturated chloride diffusion on the pore structure in cementitious materials *Cement and Concrete Research* 2020: pp. 1 – 14.
https://doi.org/10.1016/j.cemconres.2019.105919

26. **Zhang, Y., Ye, G., Yang, Z.** New insights into long-term chloride transport in unsaturated cementitious materials: Role of degree of water saturation *Construction and Building Materials* 2020: pp. 1 – 11.
https://doi.org/10.1016/j.conbuildmat.2019.117677

27. **Tang, S.W., Yao, Y., Andrade, C., Li, Z.J.** Recent durability studies on concrete structure *Cement and Concrete Research* 78 2015: pp. 143 – 154.
https://doi.org/10.1016/j.cemconres.2015.05.021

28. **Barneyback, Jr.R.S., Diamond, S.** Expression and analysis of pore fluids from hardened cement pastes and mortars *Cement and Concrete Research* 11 (2) 1981: pp. 279 – 285.
https://doi.org/10.1016/0008-8846(81)90069-7

29. **Climent, M.A., Viqueira, E., de Vera, G., López-Atalaya, M.M.** Analysis of acid-soluble chloride in cement, mortar, and concrete by potentiometric titration without filtration steps *Cement and Concrete Research* 29 (6) 1999: pp. 893 – 898.
https://doi.org/10.1016/S0008-8846(99)00063-0

30. **Zhang, Y., Ouyang, X., Yang, Z.** Microstructure-based relative humidity in cementitious system due to self-desiccation *Materials* 12 (8) 2019: pp. 1 – 15.
https://doi.org/10.3390/ma12081214

31. **Vollpracht, A., Lothenbach, B., Snellings, R., Haufe, J.** The pore solution of blended cements: a review *Materials and Structures* 49 2015: pp. 3341 – 3367.
https://doi.org/10.1617/s11527-015-0724-1

32. **Bertolini, L., Elsener, B., Pedeferri, P., Redaelli, E., Polder, R.B.** Corrosion of Steel in Concrete: Prevention, Diagnosis, Repair, John Wiley & Sons, 2013.

33. **Wang, J., Niu, D., Ding, S., Mi, Z., Luo, D.** Microstructure, permeability and mechanical properties of accelerated shotcrete at different curing age *Construction and Building Materials* 78 2015: pp. 203 – 216.
https://doi.org/10.1016/j.conbuildmat.2014.12.111

34. **Zhang, P., Wittmann, F.H., Lura, P., Mueller, H.S., Han, S., Zhao, T.** Application of neutron imaging to investigate fundamental aspects of durability of cement-based materials: A review *Cement and Concrete Research* 108 2018: pp. 152 – 166.
https://doi.org/10.1016/j.cemconres.2018.03.003